Eur. Phys. J. C 34, 157–163 (2004)
Digital Object Identifier (DOI) 10.1140/epjc/s2004-01668-9

THE EUROPEAN PHYSICAL JOURNAL C

Detection of heavy charged Higgs bosons in $e^+e^- \to t\bar{b}H^-$ production at future Linear Colliders

S. Moretti[a]

School of Physics & Astronomy, University of Southampton, Highfield, Southampton SO17 1BJ, UK

Received: 10 July 2003 / Revised version: 9 November 2003 /
Published online: 12 March 2004 –

Abstract. Heavy charged Higgs bosons ($H^\pm$) of a Type II 2-Higgs doublet model (2HDM) can be detected at future electron–positron Linear Colliders (LCs) even when their mass is larger than half the collider energy. The single Higgs mode $e^+e^- \to t\bar{b}H^- +$ c.c. $\to 4b + \mathrm{jj} + \ell + p_{\mathrm{T}}^{\mathrm{miss}}$ (where j represents a jet and with $\ell = e, \mu$) contributes to extend the discovery reach of $H^\pm$ states into the mass region $M_{H^\pm} \gtrsim \sqrt{s}/2$, where the well studied pair production channel $e^+e^- \to H^-H^+$ is no longer available. With a technique that allows one to reconstruct the neutrino four-momentum in the decay $t \to bW^+ \to b\ell^+\nu$, one can suppress the initially overwhelming main irreducible background due to $e^+e^- \to t\bar{t}b\bar{b}$ (via a gluon splitting into $b\bar{b}$ pairs) to a negligible level. However, for currently foreseen luminosities, one can establish a statistically significant $H^\pm$ signal only over a rather limited mass region, of 20 GeV or so, beyond $M_{H^\pm} \approx \sqrt{s}/2$, for very large or very small values of $\tan\beta$ and provided high b-tagging efficiency can be achieved.

Charged Higgs bosons appear in the particle spectrum of a general 2HDM. Embedding a Type II such model into the theoretical framework provided by supersymmetry (SUSY) yields the minimal supersymmetric standard model (MSSM). In the presence of SUSY, the mass of the two charged Higgs states of the theory is closely tied to that of the CP-odd neutral Higgs boson, denoted by A, and to those of the two CP-even neutral states, labelled as h and H (in increasing order of mass). These five states make up the Higgs particle spectrum of a 2HDM. The ratio of the vacuum expectation values (VEVs) of the two Higgs doublets, hereafter $\tan\beta$, together with the mass of one of the physical Higgs states (say, M_A) uniquely defines the production and decay phenomenology of the MSSM Higgs sector at tree level, provided the mass of the SUSY partners of ordinary matter (so-called sparticles) is significantly higher than the hard scale involved in the Higgs processes considered.

There exists a significant region of the MSSM parameter space, the so-called "decoupling limit", namely, when $M_A \sim M_H \sim M_{H^\pm} \gg M_h$, for values of $\tan\beta$ between, say, 2–3 and 30–40 (the larger M_A the higher the upper limit in $\tan\beta$), where only the light (below 130 GeV or so) neutral Higgs boson h is found at the Large Hadron Collider (LHC) and this is degenerate with the SM Higgs state. Under these circumstances, it would be very difficult to investigate at the LHC the mechanism of electro-weak symmetry breaking (EWSB) and understand whether the latter is generated within the SM or else by the MSSM dynamics.

The availability of e^+e^- LCs operating at the TeV scale or above [1] will then be crucial to solve this puzzle. In this respect, the accepted wisdom is that high precision measurements can easily be performed in such a clean environment, enabling one to asses the true nature of such a light Higgs state, possibly inferring also the values of M_A, M_H and $M_{H^\pm}$. In fact, mass relations among the five MSSM Higgs states are now known very accurately, at the two-loop level [2][1], as a function of $\tan\beta$, that could also be determined rather easily at LCs.

However, it may well turn out that the extrapolated mass for the heavy Higgs states of the model is larger than half the LC energy: i.e., $M_A \sim M_H \sim M_{H^\pm} \gtrsim \sqrt{s}/2$. This would be a rather difficult configuration to investigate even at LCs. In fact, this occurs when the couplings ZAh and ZZH are minimal, hence preventing one from exploiting the $e^+e^- \to Ah$ and $e^+e^- \to ZH$ production processes[2] to access the CP-odd and heavy CP-even neutral Higgs bosons. The only means of producing these objects would be via $e^+e^- \to AH$, whose cross section is maximal in the decoupling limit, yet negligible if $M_H + M_A \gtrsim \sqrt{s}/2$. Similarly, the leading production mode of charged Higgs states is via $H^\pm$ pairs, $e^+e^- \to H^-H^+$ [3], which presents the same drawbacks.

[a] e-mail: stefano@hep.phys.soton.ac.uk

[1] Recall that some virtual sparticle effects can enter such relations, even for high SUSY mass values. However, the dependence is rather mild (logarithmic, to be precise) and almost invisible for the case of the charged Higgs state, for which one may safely adopt the tree-level expression $M^2_{H^\pm} = M^2_A + M^2_{W^\pm}$.

[2] There is no ZZA coupling at tree level in the MSSM; hence the $e^+e^- \to ZA$ channel is phenomenologically irrelevant.

Clearly, the discovery of the additional Higgs states expected in the model (other than h) and the measurement of their quantum numbers is a necessary ingredient to definitely pin down the dynamics of the underlying EWSB mechanism. Despite the difficult situation outlined above, there are two strategies that one can pursue at future LCs. One can either exploit the $\gamma\gamma$ option to produce heavy neutral Higgs states in single mode, via (triangle) loops of heavy fermions (τ-leptons, but chiefly b- and t-quarks), plus possibly $W^\pm, H^\pm$ bosons (limitedly to the CP-even state), or resort to e^+e^- production modes of A, H and $H^\pm$ states that only involve one of such particles at a time. While the option of allowing for photon–photon interactions may certainly be viable (at an energy and luminosity close to those of the primary e^+e^- design), the case for the investigation of the second alternative is certainly stronger. (Besides, the $\gamma\gamma$ mode would not be helpful in the case of charged Higgs bosons.)

Heavy neutral Higgs bosons could for example be produced via $e^+e^- \to b\bar{b}A$ and $e^+e^- \to b\bar{b}H$ [4], provided $\tan\beta$ is significantly above unity. Alternatively, one could try exploiting loop production of A bosons via $e^+e^- \to \nu\bar{\nu}A$ [5]. Some investigations of these channels exist in the literature; yet a dedicated signal-to-background analysis is still missing to date. We will address this in a separate publication [6]. Here, we will concentrate on single production of charged Higgs bosons[3].

There exist several channels yielding only one $H^\pm$ state in the final state of electron–positron annihilations at TeV energy scales [9–13]. The only ones though that can offer some chances of detection are the following:

$$e^+e^- \to \tau^-\bar{\nu}_\tau H^+, \tau^+\nu_\tau H^- \quad \text{(tree level)}, \tag{1}$$

$$e^+e^- \to b\bar{t}H^+, t\bar{b}H^- \quad \text{(tree level)}, \tag{2}$$

$$e^+e^- \to W^\mp H^\pm \quad \text{(one loop)}. \tag{3}$$

The first one is relevant only in the large $\tan\beta$ region, whereas the latter is important only for the low $\tan\beta$ one. The second one can cover both, yet is of little use for intermediate $\tan\beta$ values (say, around 6–10). As LEP2 data seem to prefer large values of $\tan\beta$, at least in the MSSM [14], some attempts of disentangling the first process from the background in the mass interval $M_{H^\pm} \gtrsim \sqrt{s}/2$ were carried out in [15], and not without success. In fact, some coverage was claimed over a region extending for about 20–30 GeV above the kinematic limit $M_{H^\pm} = \sqrt{s}/2$, for $\tan\beta \gtrsim 30$–40. We attempt here to devise a selection procedure that may help to extract process (2) from the irreducible background[4]. Since, as shown in [9], the production rates for channel (2) are rather small in general over the mass region $M_{H^\pm} \gtrsim \sqrt{s}/2$ (for the sake of illustration, we adopt here $\sqrt{s} \equiv E_{\rm cm} = 1000\,\text{GeV}$), it is mandatory to resort to the main decay channel of heavy charged Higgs bosons, i.e., $H^+ \to t\bar{b}$. Hence, the following processes are of relevance for the signal (S) and the main irreducible background (B)[5]:

$$e^+e^- \to b\bar{t}H^+ + t\bar{b}H^- \to t\bar{t}b\bar{b} \quad \text{(signal)}, \tag{4}$$

$$e^+e^- \to t\bar{t}g^* \to t\bar{t}b\bar{b} \quad \text{(background)}. \tag{5}$$

We search for the two emerging top quarks in semi-leptonic (or semi-hadronic) modes, i.e.,

$$t\bar{t} \to b\bar{b}W^+W^- \to b\bar{b}\text{jj}\ell\nu, \tag{6}$$

where j identifies a light-quark jet and $\ell = e, \mu$. We assume four b-tags but no b-jet charge determination, so that the final signature is

$$4b + \text{jj} + \ell + p_{\rm T}^{\rm miss}, \tag{7}$$

as the neutrino eventually escapes detection.

However, one can actually reconstruct the longitudinal momentum of the neutrino, even in the presence of initial state radiation (ISR). The method is rather simple and it was initially outlined for the case of hadron–hadron collisions [17], where the initial boost due to the (anti)quarks and gluons scattered out of the (anti)protons can have far more severe effects on the momentum reconstruction than those due to ISR in electron–positron annihilations. We will outline the procedure below.

In our numerical results, we have assumed the MSSM throughout with M_A ranging between 120 and 660 GeV. Most of the signal plots will be presented for $\tan\beta = 40$. However, we will discuss other $\tan\beta$ values at the end. For the signal, we have used the same program employed in [9] for the production process and the one described in [18] for the branching ratios (BRs), all allowing for the inclusion of off-shellness effects of the charged Higgs bosons[6]. The other unstable particles entering the two processes, i.e., t and $W^\pm$, were also generated off-shell, with $\Gamma_t = 1.55\,\text{GeV}$ and $\Gamma_W = 2.08\,\text{GeV}$, in correspondence with $m_t = 175\,\text{GeV}$ and $M_{W^\pm} = M_Z \cos\theta_{\rm W} \approx 80\,\text{GeV}$ ($M_Z = 91.19\,\text{GeV}$ and $\sin^2\theta_{\rm W} = 0.232$). The non-running b-quark mass adopted for both the kinematics and the Yukawa coupling was $m_b = 4.25\,\text{GeV}$. We neglect ISR and beamstrahlung effects, as we expect these to have a marginal impact on the *relative* behaviour of signal and background.

The entire simulation has been carried out at parton level, by identifying jets with the partons from which they originate, though a finite calorimeter resolution has been emulated through a Gaussian smearing in transverse momentum, $p_{\rm T}$, with $(\sigma(p_{\rm T})/p_{\rm T})^2 = (0.60/\sqrt{p_{\rm T}})^2 + (0.04)^2$ for jets and $(\sigma(p_{\rm T})/p_{\rm T})^2 = (0.12/\sqrt{p_{\rm T}})^2 + (0.01)^2$ for leptons. The resulting missing transverse momentum, $p_{\rm T}^{\rm miss}$, was reconstructed from the vector sum of the visible jet/lepton momenta after resolution smearing. Finally, the integration over the final states has been performed numerically with the aid of VEGAS [20] and Metropolis [21].

[3] For similar studies in the case of $\gamma\gamma$, or even $e\gamma$, collisions, see [7, 8].

[4] We defer a similar study of channel (3) to a forthcoming publication [16].

[5] Charged conjugated (c.c.) channels are assumed throughout the paper.

[6] For the computation of the backgrounds we have used MadGraph [19].

After selecting the missing neutrino, the lepton, the b- and light-quark jets in the detector region, by imposing the following (acceptance) cuts in transverse momentum, polar angle and cone separation:

$$p_{\rm T}^{\rm miss},\ p_{\rm T}^{\ell},\ p_{\rm T}^{b},\ p_{\rm T}^{\rm j} > 5\,{\rm GeV},$$
$$|\cos\theta_\ell|,\ |\cos\theta_b|,\ |\cos\theta_{\rm j}| < 0.995,$$
$$\Delta R_{\ell b},\ \Delta R_{\ell {\rm j}},\ \Delta R_{bb},\ \Delta R_{b{\rm j}},\ \Delta R_{\rm jj} > 0.4, \qquad (8)$$

one proceeds as follows[7].
(1) The invariant mass of the two non-b-jets is required to be consistent with $M_{W^\pm}$,

$$|M_{\rm jj} - M_{W^\pm}| \leq 15\,{\rm GeV}. \qquad (9)$$

(2) The invariant mass formed by combining the untagged jet pair with one of the four b-jets is required to match m_t,

$$|M_{b{\rm jj}} - m_t| \leq 25\ {\rm GeV}. \qquad (10)$$

If several b-jets satisfy this constraint, the one giving the best agreement with m_t is selected.
(3) The neutrino momentum is reconstructed by equating $p_{\rm T}^{\nu} = p_{\rm T}^{\rm miss}$ and deducing the longitudinal component $p_{\rm L}^{\nu}$ from the invariant mass constraint $M_{\ell\nu} = M_{W^\pm}$. The resulting equation is quadratic, hence it can give two solutions. If they are complex we discard their imaginary parts so that they coalesce. Otherwise, both solutions are retained.
(4) The invariant mass formed by combining ℓ and ν with one of the three remaining b-jets is also required to reproduce m_t:

$$|M_{b\ell\nu} - m_t| \leq 25\,{\rm GeV}. \qquad (11)$$

Again, if several b-jets satisfy the above requirement, the one giving the best agreement with m_t is selected along with the corresponding value of $p_{\rm L}^{\nu}$.
(5) The remaining pair of b-jets may be looked upon as the $b\bar{b}$ pair accompanying the $t\bar{t}$ in the signal (4) and background (5). Note that one of these b-jets is expected to come from the $H^\pm$ decay in the signal, while for the background they both come from a gluon splitting. Consequently, in the latter case one supposes the $b\bar{b}$ pair to have a rather different kinematics with respect to the former. We will eventually verify and make use of such differences in order to optimise our selection[8].

We start our numerical investigation by comparing the LC rates for process (2) computed when all unstable particles (t, $W^\pm$ and $H^\pm$) are set on-shell, i.e., in the narrow width approximation (NWA), to those in which the latter are all allowed to be off-shell. The corresponding curves

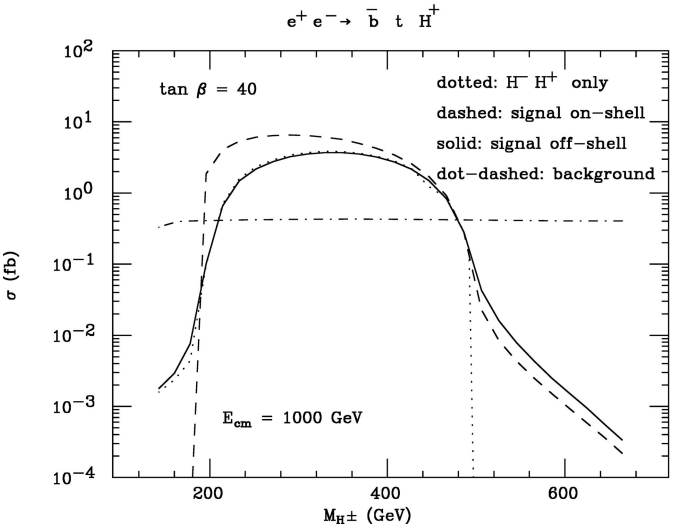

Fig. 1. Total cross sections for processes (4) and (5) yielding the signature (7), with the charged Higgs boson (and other unstable particles) being on- and off-shell, including all decay BRs. No cuts have been enforced here. We also show the cross sections corresponding to graphs proceeding via $e^+e^- \to H^-H^+$

are displayed in Fig. 1. For reference, in the same figure, we also show the rates obtained by using the two-body mode $e^+e^- \to H^-H^+$ followed by the decay $H^- \to b\bar{t}$ (including off-shell top (anti)quarks). No cuts are enforced here. At the "threshold" point $M_{H^\pm} \approx \sqrt{s}/2$, one may notice that two of the curves start departing. These contain diagrams other than those proceeding via $e^+e^- \to H^-H^+$ as well as the relative interference between the two sets of graphs. The difference between the two curves is due to the finite width of the charged Higgs boson, which is of order 10 GeV or so at 500 GeV and above. At $M_{H^\pm} \approx m_t$, one may also appreciate the effects of finite values of $\Gamma_t, \Gamma_{W^\pm}$ and $\Gamma_{H^\pm}$. We are however interested in the $M_{H^\pm} \gtrsim \sqrt{s}/2$ region. Here, one should notice that the $t\bar{t}b\bar{b}$ background (including the decay BRs yielding the final state in (7)) is about 0.40 fb (at leading order)[9]. The S/B ratio is rather small then, to start with – about 1/20 at $M_{H^\pm} \approx \sqrt{s}/2$ (recall that $\sqrt{s} = 1000\,{\rm GeV}$), yet not prohibitive to attempt disentangling the signal from the irreducible background.

We now proceed in our investigation by enforcing the acceptance and selection cuts in (8)– (11). The signal and background cross sections which survive these constraints can be found in Fig. 2 (solid and dashed lines). Despite that also the background contains two top (anti)quarks, the improvement in S/B is substantial, as, at $M_{H^\pm} \approx \sqrt{s}/2$, it has now decreased to 1/8 or so. The main cause for the severe background reduction turns out to be the separation cuts between jets, as in the $g^* \to b\bar{b}$ splitting the two emerging b-jets tend to be collinear[10].

[7] The adoption of a jet-clustering algorithm [22] instead of a cone one, as done in [15, 23], would not affect our final conclusions.

[8] Note the more conservative constraints adopted here in the $W^\pm$ and t mass reconstruction with respect to [15], which is justified by the larger hadronic multiplicity of the present final state.

[9] Here, the small drop for $M_{H^\pm}$ below m_t is due to the fact that we have not included the $t \to bH^+$ decays in the definition of the background.

[10] Note that the gluon radiated off the $t\bar{t}$ pair can be rather energetic, as $\sqrt{s} \gg 2m_t$.

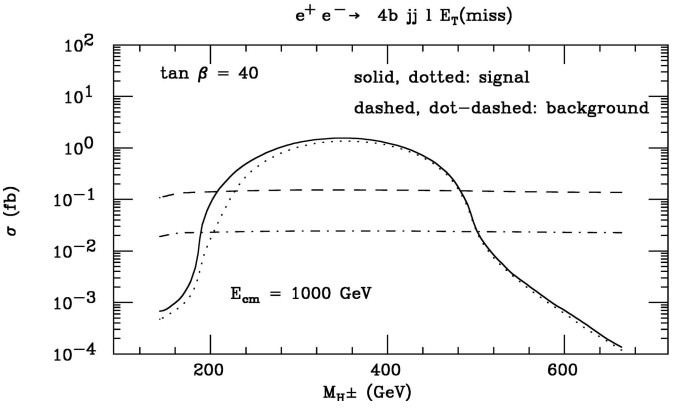

Fig. 2. Total cross sections for processes (4) and (5) yielding the signature (7), after the kinematic cuts in (8)–(11) [solid and dashed lines] and after the additional cuts in (12) [dotted and dot-dashed lines], including all decay BRs

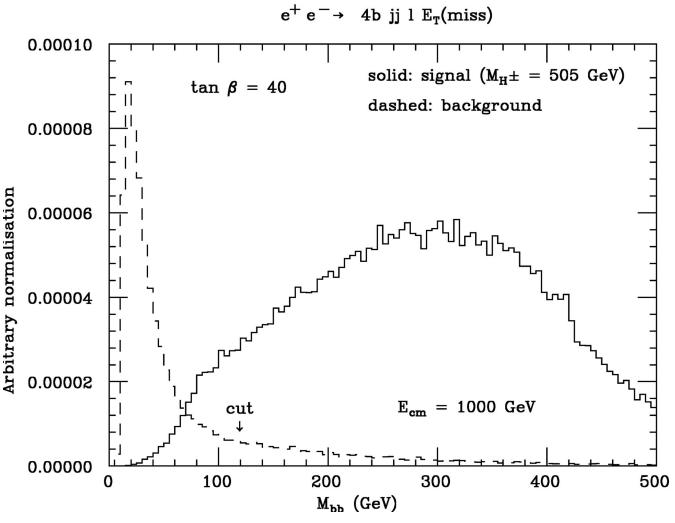

Fig. 3. Differential distribution in the invariant mass of the two b-jets not generated in top decays for processes (4) and (5) yielding the signature (7), after the kinematic cuts in (8)–(11), including all decay BRs

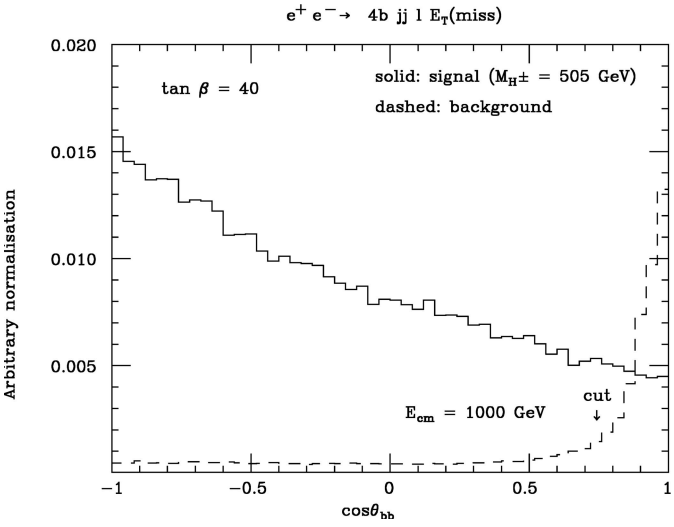

Fig. 4. Differential distribution in the relative angle of the two b-jets not generated in top decays for processes (4) and (5) yielding the signature (7), after the kinematic cuts in (8)–(11), including all decay BRs

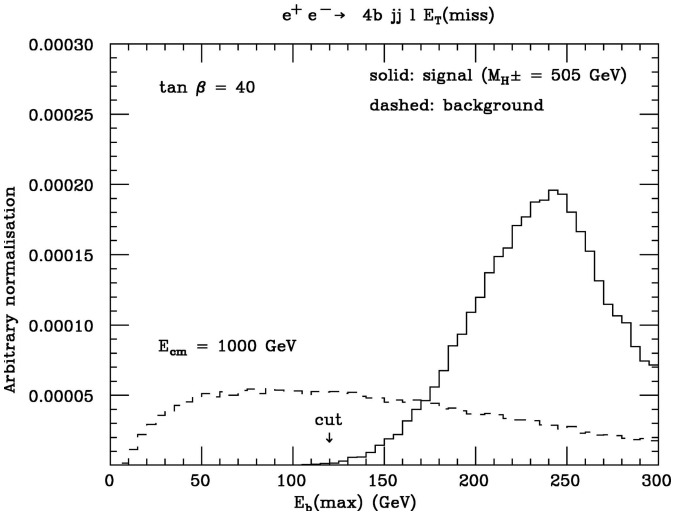

Fig. 5. Differential distribution in energy of the hardest of the two b-jets not generated in top decays for processes (4) and (5) yielding the signature (7), after the kinematic cuts in (8)–(11), including all decay BRs

An even more vigorous reduction of the background rate, especially in the very heavy Higgs mass region, can be obtained by exploiting the different kinematic behaviour of the hadronic system involving the two b-jets not associated to the reconstructed pair of top (anti)quarks, as mentioned earlier on. Figures 3–5 illustrate the dependence of signal and background rates on the three following variables: the invariant mass, M_{bb}, the (cosine of the) relative angle, $\cos\theta_{bb}$, and the energy of the hardest of the two b-jets, $E_b(\max)$. The Higgs mass in the signal has been chosen in the critical region, $M_{H^\pm} \gtrsim \sqrt{s}/2$: we have taken $M_{H^\pm} = 505\,\text{GeV}$ as an illustration. Upon investigation of Figs. 3–5, an effective combination of cuts seems to be the following:

$$M_{bb} > 120\,\text{GeV}, \quad \cos\theta_{bb} < 0.75,$$
$$E_b(\max) > 120\,\text{GeV}. \qquad (12)$$

(Note that such quantities are all correlated, so that the consequent effects do not factorise.)

The dotted and dot-dashed curves in Fig. 2 present the signal rates after the improved kinematic selection has been enforced, that is, after the implementation of the constraints in (8)– (12). (For $M_{H^\pm} > m_t$, the background cross section continues to be constant with $M_{H^\pm}$ as none of the cuts used so far depends on this parameter.) The improvement in S/B is dramatical, as the signal remains basically unaffected by the additional cuts, while the background is reduced by a factor of almost six.

After the outlined procedure has been enforced, one is in the position of being able to reconstruct the charged

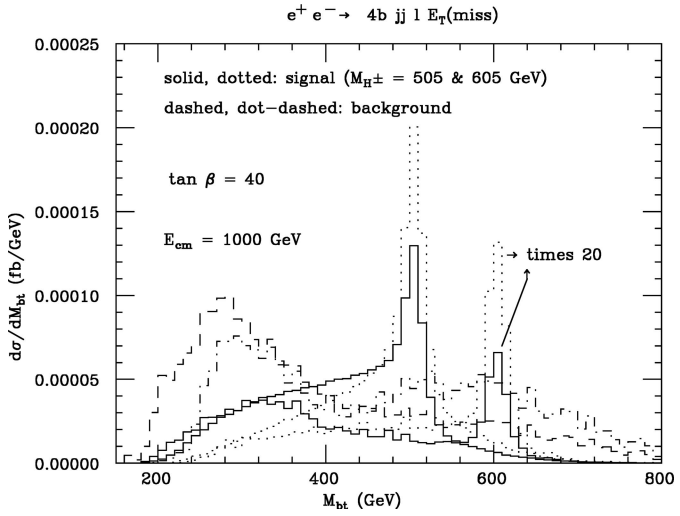

Fig. 6. (Solid and dashed lines) Differential distribution in the reconstructed Higgs mass from both b-jets not generated in top decays and the two top systems (see definition (a) in the text) for the processes (4) and (5) yielding the signature (7), after the kinematic cuts in (8)–(12), including all decay BRs. (Dotted and dot-dashed lines) Same as above, but using only the b-jet with highest transverse momentum of the two not generated in top decays (see definition (b) in the text)

Higgs boson mass. There are two possible ways to proceed in doing so.

(a) One can combine each of the reconstructed t-quarks with each of the remaining b-jets to obtain four entries for the bt invariant mass, M_{bt}. For each signal point, one of these entries will correspond to the parent $H^\pm$ mass while the other three will represent the combinatorial background. We plot the signal and background cross sections against this quantity in Fig. 6 (solid and dashed lines). The former clearly shows the resonant peak at $M_{H^\pm}$ emerging over a broad combinatorial background, while the latter presents only a rather flat distribution in M_{bt} near the signal resonances.

For $M_{H^\pm} \gg m_t$, indeed the region of our interest, one of the two spare b-jets in the signal (namely, the one coming from the $H^+ \to t\bar{b}$ decay) would generally be much harder than the other. Hence one can expect to reduce the combinatorial background as follows.

(b) One can combine each of the reconstructed t-quarks with the harder of the two accompanying b-jets. This gives two values for the invariant mass M_{bt} for each signal point, one of which corresponds to the parent $H^\pm$ mass. We show the signal and background cross sections against this quantity in Fig. 6 (dotted and dot-dashed lines). The pattern is similar to what was seen previously; yet the signal resonances are now significantly narrower.

In either case, despite that the width of the signal spectra is dominated by detector smearing effects, it is clear that the Breit–Wigner peaks themselves can help to improve S/B further as well as to determine the $H^\pm$ mass. Figure 6 suggests then that a further selection criterion can be afforded at this stage: e.g.,

$$|M_{bt} - M_{H^\pm}| < 40\,\text{GeV}. \tag{13}$$

The value of $M_{H^\pm}$ entering (13) would be the central or fitted mass resonance of the region in M_{bt} where an excess of the form seen in Fig. 6 will be established. We perform the exercise for both mass spectra (the one involving four entries and the one using two).

The resulting cross sections for signal and background, after the additional cut in (13), are shown in the top frame of Fig. 7, as obtained from the two M_{bt} distributions above. The signal rates are not very large in the $M_{H^\pm} \gtrsim \sqrt{s}/2$ region with the background ones being comparable or even higher. Yet, with the very large luminosity that can be accumulated at a future LC, statistical significances ($S/\sqrt{B}$) may be sizable. The latter are displayed, after 1 and 5 ab^{-1} of accumulated luminosity, $\mathcal{L}$, in the bottom frame of Fig. 7; again, as obtained from the two definitions of M_{bt} given in (a) and (b). (The first luminosity figure may well be attained according to current designs, while the second should be viewed at present as an optimistic scenario.) By comparing these curves with the shape of the $e^+e^- \to H^-H^+$ cross section in Fig. 1, one should expect to be able to extend the reach in $M_{H^\pm}$ obtained from pair production of charged Higgs bosons and decays by at most 25 GeV at 3σ level above the $M_{H^\pm} = \sqrt{s}/2$ point and only at very high luminosity, thanks to the contribution of single $H^\pm$ production in association with top- and bottom-(anti)quarks. Typical signal rates at $\tan\beta = 40$ in the threshold region $M_{H^\pm} \approx \sqrt{s}/2$ would be about 5(25) events for definition (a) of M_{bt} and 7(35) for (b), in correspondence with $\mathcal{L} = 1(5)$ ab^{-1}.

However, recall that process (2) is very sensitive to the actual value of $\tan\beta$. While in the $\tan\beta \gtrsim 40$ region its production rates approximately scale like $\tan\beta^2$ (so that the higher this parameter the better the chances of isolating the signal discussed here, though a natural upper limit for it is expected at around 50), for $\tan\beta$ much smaller than 40 the statistical significance would diminish very rapidly, unless $\tan\beta$ values of order 1.5 or so are allowed within the underlying model. In fact, the average strength of the $t\bar{b}H^-$ coupling is proportional to $\sqrt{m_t^2 \cot\beta^2 + m_b^2 \tan\beta^2}$, which has a minimum at $\tan\beta \approx \sqrt{m_t/m_b} \approx 6.4$. Figure 8 illustrates this trend, for the more realistic value of luminosity, $\mathcal{L} = 1\,\text{ab}^{-1}$, and limited to the kinematically more favourable case in which M_{bt} is computed as described in case (b) above. Under these conditions, the maximum mass reach at 3σ level beyond the threshold region $M_{H^\pm} \sim \sqrt{s}/2$ is of order 20 GeV or so, for very large or very small $\tan\beta$. Finally, in our estimates so far, we have excluded the efficiency of tagging the four b-jets in the final state. According to [23], the single b-tag efficiency is expected to be close to the value $\epsilon_b = 90\%$, thus yielding – if all four b-quarks are tagged – a reduction factor of $\epsilon_b^4 \approx 0.66$ for the number of events of both signal and background and of $\epsilon_b^2 \approx 0.81$ for the statistical significance $S/\sqrt{B}$, hence diminishing even further the scope of our signature. Eventually, the impact of the next-to-leading order QCD corrections computed in [24] should also be evaluated carefully, as they can alter

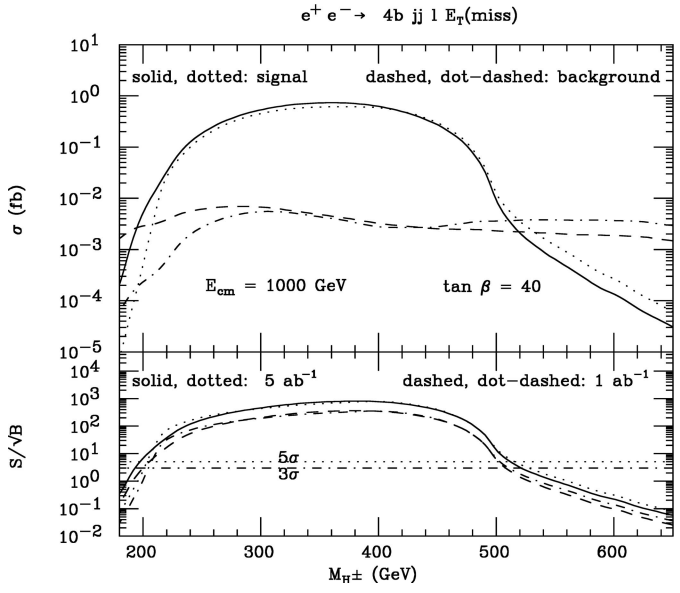

Fig. 7. (Top) Total cross sections for processes (4) and (5) yielding the signature (7), after the kinematic cuts in (8)–(12) plus the one in (13) applied to the M_{bt} distribution defined in (a) [solid and dashed lines] and in (b) [dotted and dot-dashed lines] (see the text), including all decay BRs. (Bottom) Corresponding statistical significances of the signal for two values of integrated luminosity (the 3σ and 5σ "evidence" and "discovery" thresholds are also given)

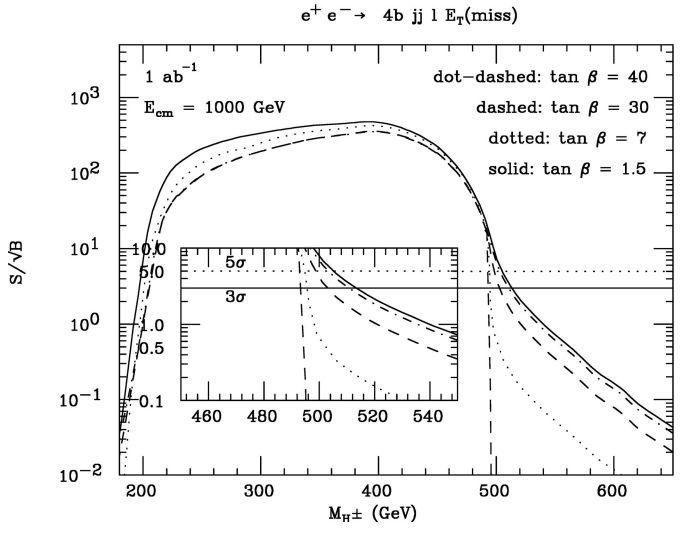

Fig. 8. Statistical significances of the signal (4) yielding the signature (7), after the kinematic cuts in (8)–(12) plus the one in (13) applied to the M_{bt} distribution defined in (b) (see the text), including all decay BRs, for four different values of $\tan\beta$. The value of integrated luminosity is here $1\,\mathrm{ab}^{-1}$ (the 3σ and 5σ "evidence" and "discovery" thresholds are also given). The vertical dashed line corresponds to the kinematic limit of the graphs proceeding via $e^+e^- \to H^-H^+$ (see also Fig. 1). In the insert, we enlarge the region $M_{H^\pm} \sim \sqrt{s}/2$

the leading order results for the signal by up to $\pm 50\%$, depending on the values of $\sqrt{s}$, $M_{H^\pm}$ and $\tan\beta$. We refrain from doing so here for consistency, as the irreducible background that we have considered would also be subject to large QCD effects, which are however still unknown.

In summary, while not having been very encouraging per se, if combined with the results of [9–13] and [15, 25] for the $\tau^-\bar{\nu}_\tau H^+$ and W^-H^+ channels, our present findings should be taken into account in establishing strategies to detect heavy charged Higgs bosons with masses $M_{H^\pm} \gtrsim \sqrt{s}/2$ at future LCs, especially considering the very high level of background reduction achieved through our kinematic selection, which started from very poor S/B rates. Unfortunately, absolute rates for singly produced heavy $H^\pm$ states are never very large either, so that to achieve a high luminosity is of paramount importance. Our conclusions have been derived within the MSSM, nonetheless, they are equally applicable to a general Type II 2HDM, as the only couplings involved in the present analysis are common to both scenarios. In particular, in a 2HDM the mentioned low $\tan\beta$ region is not excluded, so that also in this framework the $b\bar{t}H^+$ channel may well turn out to be of use.

Two ways for further work can be foreseen to be the following. On the one hand, one can attempt to exploit process (3) in order to cover the same kinematic region at low to intermediate $\tan\beta$ [16]. On the other hand, one ought to eventually fold the parton level results into a more sophisticated simulation, as we are planning to do [6] in the context of the HERWIG Monte Carlo event generator [26, 27], where more realistic estimates for b-tagging efficiency and rejection against mis-identification of light-quark and gluon jets would be obtained. In this context, one may also consider the possibility of tagging three b-jets only, which would still allow for the implementation of the kinematic selection outlined here, at the same time increasing somewhat both the signal rates and significances while not implying additional backgrounds, as b-quarks are always produced in pairs in e^+e^- annihilations.

Acknowledgements. We thank Bernd Kniehl for encouragement to pursue this work and for illuminating discussions.

References

1. K. Abe et al. [The ACFA Linear Collider Working Group], hep-ph/0109166 and references therein; T. Abe et al. [The American Linear Collider Working Group], hep-ex/0106055; hep-ex/0106056; hep-ex/0106057; hep-ex/0106058 and references therein; J.A. Aguilar-Saavedra et al. [The ECFA/DESY LC Physics Working Group], hep-ph/0106315; G. Guignard (editor), [The CLIC Study Team], preprint CERN-2000-008
2. S. Heinemeyer, W. Hollik, G. Weiglein, Eur. Phys. J. C **9**, 343 (1999)
3. S. Komamiya, Phys. Rev. D **38**, 2158 (1988)
4. K.J.F. Gaemers, G.J. Gounaris, Phys. Lett. B **77**, 479 (1978)
5. T. Farris, J.F. Gunion, H.E. Logan, S. Su, Phys. Rev. D **68**, 075006 (2003)
6. S. Moretti, in preparation
7. S. Kanemura, S. Moretti, Eur. Phys. J. C **29**, 19 (2003)

8. S. Kanemura, S. Moretti, K. Odagiri, Eur. Phys. J. C **22**, 401 (2001)
9. A. Djouadi, J. Kalinowski, P.M. Zerwas, Z. Phys. C **54**, 255 (1992); S. Kanemura, S. Moretti, K. Odagiri, JHEP **02**, 011 (2001); B.A. Kniehl, F. Madricardo, M. Steinhauser, Phys. Rev. D **66**, 054016 (2002)
10. S. Kanemura, S. Moretti, K. Odagiri, hep-ph/0101354; S. Kiyoura, S. Kanemura, K. Odagiri, Y. Okada, E. Senaha, S. Yamashita, Y. Yasui, hep-ph/0301172
11. A. Gutierrez-Rodriguez, O.A. Sampayo, hep-ph/9911361
12. H.E. Logan, S. Su, Phys. Rev. D **66**, 035001 (2002); D **67**, 017703 (2003)
13. S.H. Zhu, hep-ph/9901221; S. Kanemura, Eur. Phys. J. C **17**, 473 (2000); A. Arhrib, M. Capdequi-Peyranère, W. Hollik, G. Moultaka, Nucl. Phys. B **581**, 34 (2000)
14. For a review, see, e.g.: M. Antonelli, S. Moretti, hep-ph/0106332 and references therein
15. S. Moretti, Eur. Phys. J. direct C **4**, 15 (2002); hep-ph/0209210
16. S. Kanemura, S. Moretti, in preparation
17. V. Barger, R.J.N. Phillips, D.P. Roy, Phys. Lett. B **324**, 236 (1994); D.J. Miller, S. Moretti, D.P. Roy, W.J. Stirling, Phys. Rev. D **61**, 055011 (2000); S. Moretti, D.P. Roy, Phys. Lett. B **470**, 209 (1999)
18. S. Moretti, W.J. Stirling, Phys. Lett. B **347**, 291 (1995); Erratum, B **366**, 451 (1996)
19. T. Stelzer, W.F. Long, Comput. Phys. Commun. **81**, 357 (1994)
20. G.P. Lepage, J. Comput. Phys. **27**, 192 (1978)
21. H. Kharraziha, S. Moretti, Comput. Phys. Comm. **127**, 242 (2000); Erratum, B **134**, 136 (2001)
22. L. Lönnblad, S. Moretti, T. Sjöstrand, JHEP **08**, 001 (1998)
23. M. Battaglia, A. Ferrari, A. Kiiskinen, T. Maki, hep-ex/0112015
24. B.A. Kniehl, F. Madricardo, M. Steinhauser, in [9]
25. S. Kiyoura, talk given at the International Workshop on Linear Colliders (LCWS 2002), Jeju Island, Korea, 26–30 August 2002 (unpublished)
26. G. Marchesini, B.R. Webber, G. Abbiendi, I.G. Knowles, M.H. Seymour, L. Stanco, Comput. Phys. Commun. **67**, 465 (1992); G. Corcella, I.G. Knowles, G. Marchesini, S. Moretti, K. Odagiri, P. Richardson, M.H. Seymour, B.R. Webber, JHEP **01**, 010 (2001)
27. S. Moretti, K. Odagiri, P. Richardson, M.H. Seymour, B.R. Webber, JHEP **04**, 028 (2002); S. Moretti, hep-ph/0205105